




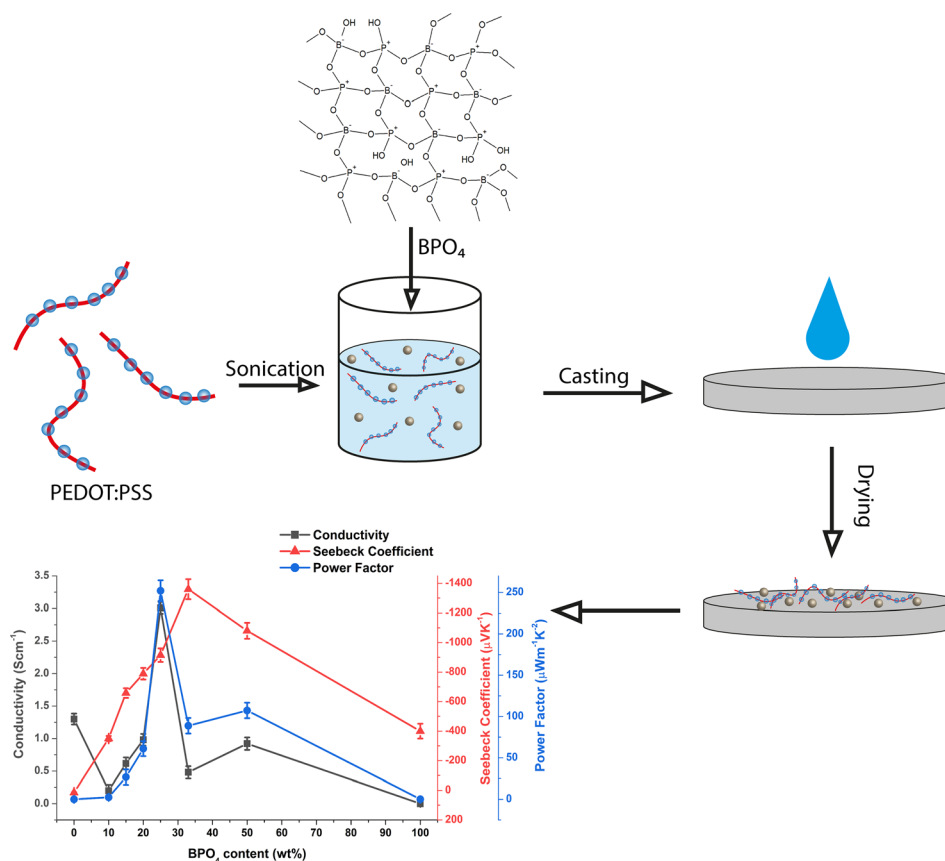
Thermoelectric Properties of n-type PEDOT:PSS/Boron Phosphate Hybrid Composites

VOLKAN UGRASKAN ^{1,2} and FERDANE KARAMAN^{1,3}

1.—Department of Chemistry, Yildiz Technical University, Istanbul 34220, Turkey. 2.—e-mail: ugraskan@yildiz.edu.tr. 3.—e-mail: ferdanekaraman@yahoo.com

In the present study, thermoelectric properties of composites formed by poly (3,4-ethylenedioxy thiophene):poly (styrene-4-sulfonate) (PEDOT:PSS)/boron phosphate (BPO_4) were studied. First, BPO_4 was synthesized at 1000°C using boric acid and phosphoric acid as precursors. Later, PEDOT:PSS was synthesized by oxidative chemical polymerization reaction at room temperature. Their composites were prepared in different mass ratios by ultrasonic homogenization. The composites were characterized using ultraviolet–visible (UV–vis.), attenuated total reflection accessory attached Fourier transform infrared (FTIR-ATR) spectroscopy, X-ray diffraction (XRD), and scanning electron microscopy/energy dispersive X-ray analyzer (SEM–EDX). The power factor of the sample was obtained using the electrical conductivity and Seebeck coefficient measurements. The positive sign of Seebeck coefficient of the pristine PEDOT:PSS turned to the negative, which is the characteristic of *n-type* material, by addition of BPO_4 . The power factor of PEDOT:PSS was increased from $0.03 \mu\text{Wm}^{-1} \text{K}^{-2}$ to $252 \mu\text{Wm}^{-1} \text{K}^{-2}$ for the composite containing 25% BPO_4 by weight. This indicates that BPO_4 can be a good additive to prepare *n-type* TE material.

Graphic Abstract



Key words: PEDOT:PSS, thermoelectric, boron phosphate, hybrid composite

INTRODUCTION

Thermoelectric (TE) power generation is an easy way to convert thermal energy directly to electrical energy.¹ TE generators have very attractive features such as light weight, low noise level, long lifetime and non-polluting for the environment. As global warming has increased, interest in TE generators, which consume waste heat, has increased, and therefore, the need to prepare efficient TE materials has increased significantly in recent years. The energy conversion efficiency of TE material is determined by the dimensionless figure of merit:

$$ZT = S^2 \sigma T / \kappa \quad (1)$$

where σ , S , κ , and T are related to electrical conductivity, Seebeck coefficient, thermal conductivity, and absolute operating temperature, respectively (Eq. 1).²⁻⁴

A TE generator is fabricated using *p*- and *n*-type TE material pairs. The main charge carriers of *p*-type materials are holes, while those of *n*-types are electrons. Although there has been a great improvement in *p*-type materials recently, *n*-type materials are far behind compared to their counterparts due to their electron trapping problem.⁵

The traditional TE materials developed since the 1950s to the present are generally inorganic compounds including metal chalcogenides (PbTe, Bi₂Te₃),^{6,7} metal oxides (Na_xCoO₂, ZnO),^{8,9} and silicon-based materials (SiGe, Mg₂Si).^{10,11} Although inorganic TE materials have high ZT values, their use is limited because of the high cost, stiffness, toxicity, scarcity, and poor processability.¹² Because of these disadvantages, many researchers focused on the development of polymeric TE materials, which are thought to overcome these drawbacks.

Conductive polymers are attractive as candidates for TE materials due to their low cost, good electrical conductivity, low thermal conductivity,

flexibility and applicability in a wide range of applications.^{13,14} The main parameter used to determine the TE performance for polymers is the power factor ($PF = S^2\sigma$) instead of ZT. This is because measurement of the thermal conductivity of polymers is challenging and their thermal conductivity is low, close to each other, and do not change significantly with inorganic additives ($0.1\text{--}0.3\text{ Wm}^{-1}\text{ K}^{-1}$).^{15,16} Although the most promising conductive polymer is poly (3,4-ethylenedioxy thiophene):poly (styrene-4-sulfonate) (PEDOT:PSS), its power factor of is not high enough.

Hybrid composites stand out as important materials due to the ability to produce high TE performance materials by combining the superior properties of the conductive polymers and inorganics. The addition of inorganic TE materials can increase TE performance since they have relatively better Seebeck coefficients compared to conductive polymers. To improve the TE performance of PEDOT-PSS, several composites were synthesized using inorganic TE materials such as Bi_2Te_3 ⁴ and Te¹⁷ or oxides such as $\text{Ca}_3\text{Co}_4\text{O}_9$ ¹⁸ and sulfides such as $\text{Cu}_{1.8}\text{S}$ ¹⁹ and TiS_2 .²⁰ However, Bi and Te are increasingly scarce and expensive, whereas the stability of TiS_2 is not long enough at ambient conditions since it is sensitive to heat, moisture and oxygen in atmosphere. Therefore, there is still a need to find polymeric TE materials including inorganic particles which are abundant, sustainable, inexpensive and stable at ambient conditions.

Among the inorganic additives, boron rich compounds have a potential to be used as a TE material because of their stability even in corrosive and acidic conditions at high temperature.²¹ Chen et al. reported that the Seebeck coefficient of hexagonal boron nitride/graphene composites reached from $50\text{ }\mu\text{VK}^{-1}$ up to $-99.3\text{ }\mu\text{VK}^{-1}$ by the addition of boron nitride.²² Wang et al. reported that the addition of boron nitride nanosheet (BNN) layers increased the power factor of PEDOT:PSS from $45.1\text{ }\mu\text{W m}^{-1}\text{ K}^{-2}$ to $100.1\text{ }\mu\text{Wm}^{-1}\text{ K}^{-2}$.²³ Moreover, the high melting points of boron compounds provide superiority to all other semiconductors and can operate at high temperatures.²⁴

BPO_4 is an isomorphous with β -cristobalite structured boron compound that is synthesized by heating a mixture of boric acid and phosphoric acid at temperatures between 25°C and 1000°C .²⁵ It is stable when the synthesis temperature is above 600°C and it is not affected by moisture but it can be dissolved in water if it is synthesized at lower temperatures. Mikhailenko et al., reported that the conductivity of BPO_4 in water was between 10^{-3} and 10^{-2} Scm^{-1} .²⁶

In the present study, we studied the change of TE properties of PEDOT:PSS with BPO_4 to obtain a stable TE material that can be used around room temperature.

MATERIALS AND METHODS

Materials

3,4-ethylenedioxythiophene (EDOT) (97%) was purchased from Acros Chemicals. Poly (styrene-4-sulfonate) (PSS) ($M_w \sim 70,000$, 30 wt. % in H_2O), ammonium persulfate (APS) (98%) and o-phosphoric acid (H_3PO_4) (85%) were purchased from Merck, Germany. Boric acid (H_3BO_3) (min. 99.9%), was purchased from ETİ Maden, Turkey.

Synthesis of BPO_4

BPO_4 was synthesized as described in the literature.²⁵ Boric acid and o-phosphoric acid were used as precursors with B/P mole ratio of 1:1.4. Appropriate amounts of H_3BO_3 and H_3PO_4 were stirred at 90°C until white creamy foam appears. After that, the mixture was heated at 1000°C for 24 h. The obtained white powder was washed with hot distilled water to remove impurities and dried in an oven at 60°C .

Synthesis of PEDOT:PSS

The polymerization of EDOT was conducted in the presence of PSS. First, 3.3 mL of PSS solution was added to 40 mL of distilled water. This was followed by the addition of 0.375 mL EDOT (3.5 mmol) to the solution so that EDOT:PSS mass ratio was 1:2. Polymerization was accomplished by adding dropwise 10 mL of ammonium persulfate solution to the mixture. (EDOT:APS mole ratio is 1:2). After the reaction proceed at ambient conditions for 16 h, PEDOT:PSS was obtained as a dark blue solution. Polymer solution was purified with ion-exchange resin to remove impurities and filtered $0.45\text{ }\mu\text{m}$ PVDF syringe filter.

Preparation of PEDOT:PSS/ BPO_4 Composites

PEDOT:PSS/ BPO_4 composites were prepared by ultrasonic homogenization to contain 10%, 15%, 20%, 25%, 33%, and 50% BPO_4 by mass. The composite films were prepared on glass substrates by drop-casting from a suspension containing 1.0%

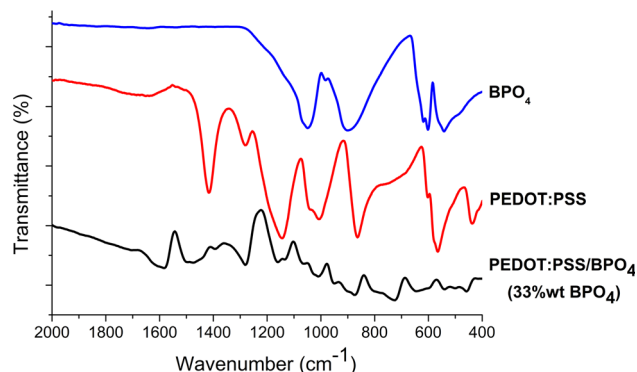


Fig. 1. FTIR-ATR spectra of BPO_4 , pristine PEDOT:PSS and PEDOT:PSS/ BPO_4 composite with 33% BPO_4 .

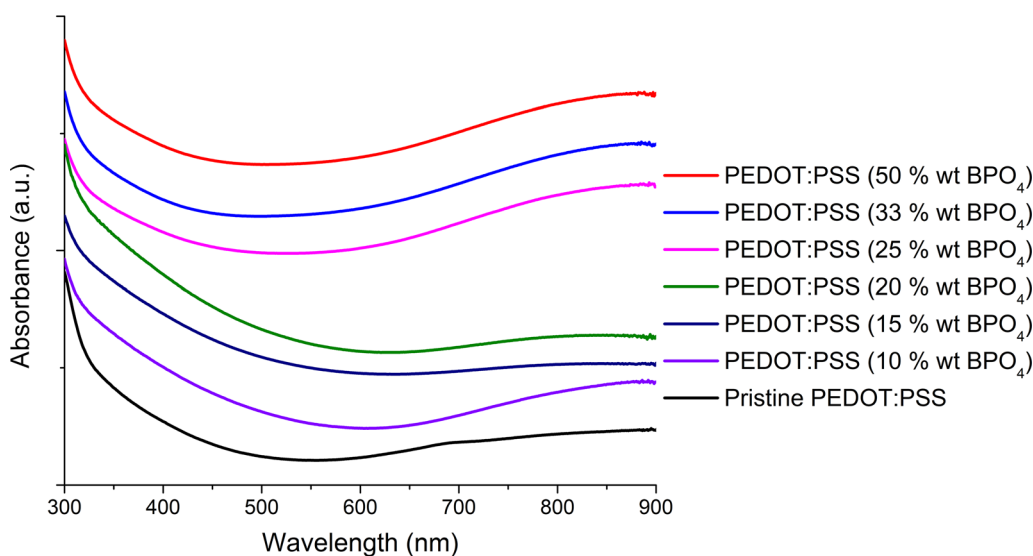


Fig. 2. UV-vis spectra of pristine PEDOT:PSS and PEDOT:PSS/BPO₄ composites in the ratios given in the label.

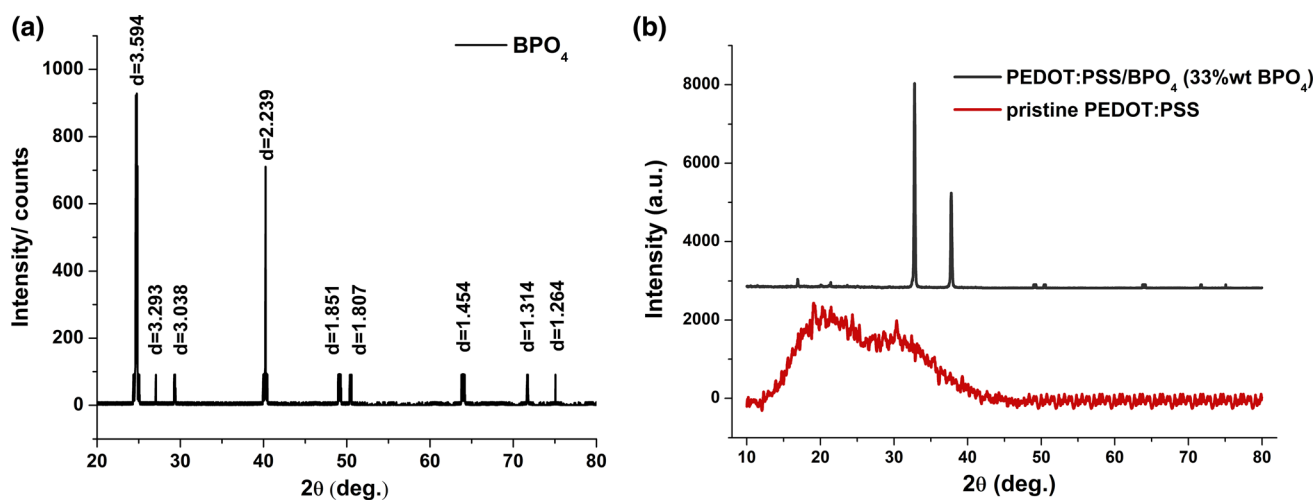


Fig. 3. XRD spectra of BPO₄, pristine PEDOT:PSS, and PEDOT:PSS/BPO₄ composite with 33% BPO₄.

solid by mass in water. Before the casting process, the glass substrates (2.5×2.5 cm) were washed with piranha solution, acetone and distilled water, respectively. Finally, composite films were dried in an oven under vacuum at 50°C for 12 h.

Characterization

The samples were characterized by FTIR (Thermo Fisher Scientific Nicolet IS10) and UV-vis (Shimadzu UVmini-1240) spectra. The crystalline structure of the samples were obtained by using XRD with Cu K α radiation ($\lambda = 1.54$ Å) (T&T TT-90 X-ray diffractometer, operated at 30 mA and 40 kVP MAX). Silicon wafer substrates were used for the deposition of the samples. The distribution of the elements in the composites was investigated by scanning electron microscopy with energy dispersive X-ray spectrometry (SEM-EDX) (Zeiss EVO[®]

LS 10). Conductivity and Seebeck coefficient measurements were carried out using an FPP 470 model four-point probe (Entek Electronic, Turkey) and Seebeck coefficient measuring device (Entek Electronic, Turkey).

RESULTS AND DISCUSSION

The FTIR-ATR spectra of BPO₄, PEDOT:PSS and the composite with PEDOT:PSS/BPO₄ with 33% BPO₄ are shown in Fig. 1. For BPO₄, the peaks in the range of 1100 – 1000 cm^{-1} are assigned to asymmetric tetrahedral B-O stretching while the peaks at around 600 cm^{-1} belong to O-B-O bending.²⁷

In the spectrum of the composite, the adsorption band at 1580 cm^{-1} corresponds to C=C stretching of the phenyl side group of PSS and the quinoid groups of PEDOT at 1492 cm^{-1} while the bands at 1290 cm^{-1} and 876 cm^{-1} are assigned to C=C, C-

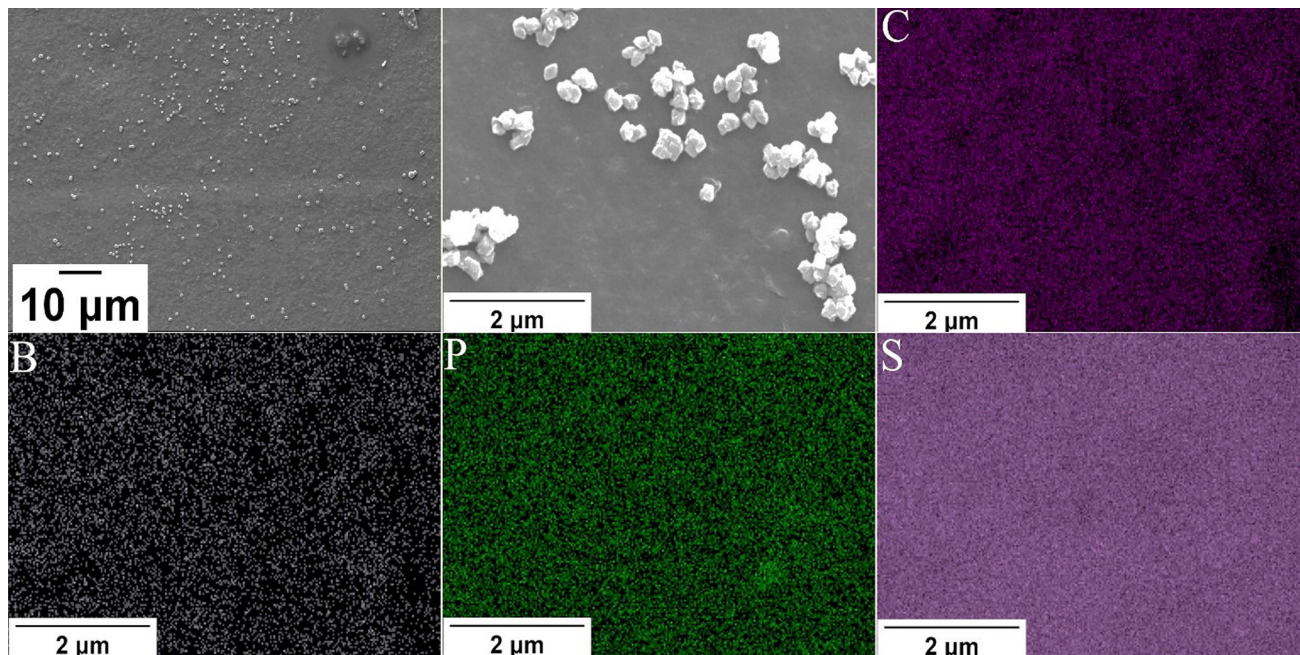


Fig. 4. SEM and EDX mapping images of PEDOT:PSS/BPO₄ with 33% BPO₄ by weight.

Table I. EDX spectra of PEDOT:PSS composite with 33% BPO₄ by weight

Element	Theoretical (wt%)	Experimental (wt%)
Boron	3.4	4
Phosphorous	9.8	12
Carbon	51.5	46
Sulphur	19.5	18

C, and C-S stretching of the thiophene ring, respectively,²⁸ whereas the bands at 1180 cm⁻¹ and 1030 cm⁻¹ belong to S-O and S-phenyl stretching.²⁹ With the addition of BPO₄, the peaks at of C=C, C-C, and C-S at 1492 cm⁻¹, 1290 cm⁻¹ and 876 slightly shifted to higher wavenumbers (blue-shift) compared to pristine PEDOT:PSS. These shifts may indicate the interfacial interaction between the polymer matrix and BPO₄.³⁰ Therefore, it can be stated that the composites are stable because of the blueshift.

The UV-vis spectra of pristine PEDOT:PSS and the composites are illustrated in Fig. 2. The concentrations of the each samples in the aqueous solution were kept the same during analyses. The curves were artificially shifted upwards to be seen more clearly. In the PEDOT:PSS spectrum, neutral and polaron regions show bands at 600 and 900 nm, respectively, while the bipolarone state shows a band around 1200 nm in the NIR region.^{31,32} In the spectra, it can be seen that the composites with 50%, 33%, and 25% BPO₄ have absorption bands tailing up to 900 nm. This broad band increasing to 900 nm represents polaron transitions, called the free

carrier tail. The transfer of the band from between 400-600 nm towards 900 nm indicates an increase in conductivity. The peak intensities of polaron bands of the composites increase considerably compared to pristine PEDOT:PSS by the addition of sufficient BPO₄. It can be stated that BPO₄ acts as a dopant for PEDOT:PSS since the amount of delocalized polarons is increased considerably with the addition of BPO₄.

The XRD patterns given in Fig. 3 are used to determine the crystalline structure of the samples synthesized in this study. Sharp peaks are observed at 24.75°, 27.05°, 29.36°, 40.23°, 49.16°, 50.44° and 63.95° in the spectrum of BPO₄ given in Fig. 3a. The peak positions are in good agreement with the XRD pattern of the standard BPO₄.³³ This reveals the purity of the BPO₄ synthesized in this study.

The crystallite size and structure of BPO₄ particles were determined using the Scherrer formula

$$\tau = \frac{k\lambda}{\beta \cos \Theta} \quad (2)$$

where τ , k , λ , Θ , and β correspond to crystallite size, the shape factor (0.9), the X-ray wavelength, the

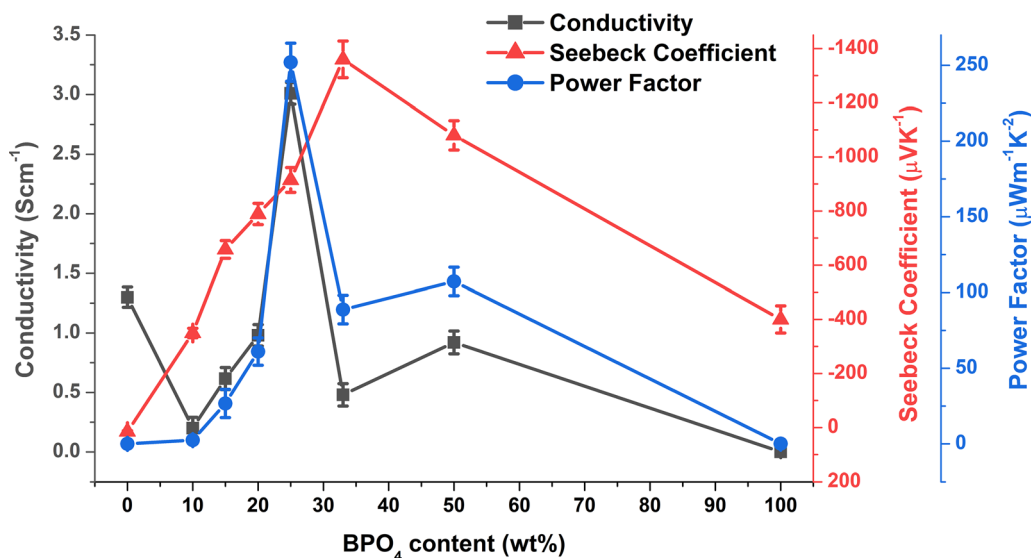


Fig. 5. Conductivity, Seebeck coefficient and power factor of BPO₄, pristine PEDOT:PSS and PEDOT:PSS/BPO₄ composites at various compositions.

Table II. Seebeck coefficients and power factors of some hybrid composites in literature

Polymer	Additive	Type	Seebeck coefficient (μVK ⁻¹)	Power factor (μWm ⁻¹ K ⁻²)	References
PEDOT:PSS	–	<i>p</i>	14.6	0.03	This study
PEDOT:PSS	BPO ₄ (33%)	<i>n</i>	– 1360	88.8	This study
PEDOT:PSS	BPO ₄ (25%)	<i>n</i>	– 915	252	This study
PEDOT:PSS	HCl Rinsing of Bi ₂ Te ₃	<i>n</i>	~ – 120	~ 80	4
Polyvinylidene Fluoride (PFDF)	Cu _{0.1} Bi ₂ Se ₃	<i>n</i>	– 84	103.2	37
Poly(vinylidene fluoride)	Bi ₂ Se ₃	<i>n</i>	– 90	40.1	37
Poly(vinylidene fluoride)	Ni	<i>n</i>	– 20.6	220	38
PEDOT:PSS	TiS ₂	<i>n</i>	– 1080	1516	20
PEDOT:PSS	Cu _{1.8} S	<i>p</i>	7000	2646	19
PEDOT:PSS	Te	<i>p</i>	114.97	284	13
PEDOT:PSS	Sb ₂ Te ₃	<i>p</i>	~ 130	336	39
PEDOT:PSS	Bi ₂ Te ₃	<i>p</i>	~ 150	130	4
PEDOT:PSS	Te	<i>p</i>	~ 200	~ 110	40
PEDOT:PSS	Ge	<i>p</i>	398	154	41
PEDOT:PSS	Te NWs	<i>p</i>	163	70.9	17

Bragg angle and the FWHM in radians.³⁴ The crystal structure of BPO₄ was found to be tetragonal with unit cell parameters $a = 4.332 \pm 0.01$ Å and $c = 6.640 \pm 0.01$ Å (JCPDS card No: 00-034-0132).²⁷ The average grain size of BPO₄ was found to be 54.06 nm according to the Scherrer formula.

It was reported that a power factor can be enhanced by adding nano-particles into the conducting polymers.³⁵ Therefore, composites are expected to show better TE performance compared to pristine PEDOT:PSS.

In the spectrum of the composite (Fig. 3b), two sharp and intense peaks appeared at 32.74° and

37.78°, whereas an amorphous halo of PEDOT:PSS disappeared. The peaks at 32.74° and 37.78° may indicate the crystallinity of PEDOT as a result of layered stacking of the polymer chains under the effect of BPO₄.³⁶

SEM–EDX mapping images of PEDOT:PSS/BPO₄ composite with 33% BPO₄ were illustrated in Fig. 4. SEM image shows that the BPO₄ in the composite is in the form of crystal particles. EDX mapping images were given to reveal the distribution of B, C, P, and S atoms in the composites. The images indicate that the elements of both components were distributed homogeneously. In addition, the

homogeneous distribution of B and P proves that BPO₄ particles in the composite are evenly dispersed. The percentage of the elements in the composition from EDX experimental data is given in Table I together with that calculated theoretically.

The conductivity was measured at room temperature while the Seebeck coefficient was measured such that the temperatures of the two ends of the samples were 293 and 343 K. Then, the power factor of the samples was calculated as a product of the conductivity and squared of the Seebeck coefficient. The values of measured conductivity and Seebeck coefficient and the calculated power factor were given in the Fig. 5.

The conductivity and Seebeck coefficient of pristine PEDOT:PSS are 1.25 Scm⁻¹ and 14.6 μVK^{-1} , respectively. Among the measured conductivity values, the highest one was 3.01 Scm⁻¹ which belongs to the composite with 25% BPO₄. All the composites have negative Seebeck coefficients specific to *n-type* semiconductors, which may be due to the behavior of phosphorus atoms in BPO₄ as *n-type* dopant for PEDOT:PSS. Among the samples, the largest Seebeck coefficient was measured as -1360 μVK^{-1} for the composite containing 33% BPO₄. The conductivity and the Seebeck coefficient values of the same samples remained unchanged for two months. The large Seebeck coefficient significantly affects the TE properties of the material since power factor is a value that increases in proportion to the square of the Seebeck coefficient. For this reason, all analyses were applied to the sample showing the highest Seebeck coefficient. In general, as the charge carrier concentration increases, the electrical conductivity increases, but the Seebeck coefficient decreases due to the interdependence between conductivity and Seebeck coefficient.³ The results given in Fig. 5 conform to this relationship except for composites containing 10% to 25% BPO₄. The calculated power factor increased from 0.03 $\mu\text{Wm}^{-1}\text{K}^{-2}$ for pristine PEDOT:PSS to 252 $\mu\text{Wm}^{-1}\text{K}^{-2}$ which belongs to the composite containing 25% BPO₄. A comparison of the Seebeck coefficients and power factors obtained in this study with the data reported for the composites of PEDOT:PSS and some fluorinated polymers in the literature is given in Table II. Among the *n-type* composites in Table II, it is seen that the largest Seebeck coefficient is -1360 μVK^{-1} , which belongs to the composite containing 33% BPO₄ prepared in this study.

CONCLUSION

The conductivity of the pristine PEDOT:PSS increased from 1.25 Scm⁻¹ to the highest value of 3.01 Scm⁻¹ with the addition of 25% BPO₄ by weight.

While pristine PEDOT:PSS was *p-type*, composites obtained by adding BPO₄ changes to *n-type* material. More specifically, the Seebeck coefficient

of pristine PEDOT:PSS changes from 14.6 μVK^{-1} to -1360 μVK^{-1} which is the largest value obtained for the composite with 33% BPO₄ by weight.

The power factor of pristine PEDOT:PSS is enhanced from 0.03 $\mu\text{Wm}^{-1}\text{K}^{-2}$ to 252 $\mu\text{Wm}^{-1}\text{K}^{-2}$ by addition of 25% BPO₄ by weight. In other words, the power factor of pristine PEDOT:PSS can be enhanced more than three orders of magnitude by adding 25% BPO₄ by weight.

Finally, by adding BPO₄, it is possible to produce stable, non-toxic, inexpensive and sustainable *n-type* PEDOT:PSS-based TE composite materials.

CONFLICT OF INTEREST

The authors declare that they have no conflict of interest.

REFERENCES

1. L. Chen, F. Meng, and F. Sun, *Sci. China Technol. Sci.* 59, 442 (2016).
2. W.B. Chang, H. Fang, J. Liu, C.M. Evans, B. Russ, B.C. Popere, S.N. Patel, M.L. Chabiny, and R.A. Segalman, *ACS Macro Lett.* 5, 455 (2016).
3. H. Yao, Z. Fan, H. Cheng, X. Guan, C. Wang, K. Sun, and J. Ouyang, *Macromol. Rapid Commun.* 39, 1700727 (2018).
4. B. Zhang, J. Sun, H.E. Katz, F. Fang, R.L. Opila, and A.C.S. Appl. *Mater. Interfaces* 2, 3170 (2010).
5. C. Gao, Y. Liu, Y. Gao, Y. Zhou, X. Zhou, X. Yin, C. Pan, C. Yang, H. Wang, G. Chen, and L. Wang, *J. Mater. Chem. A* 6, 20161 (2018).
6. Y. Gelbstein, Z. Dashevsky, and M. Dariel, *Physica B Condens. Matter* 363, 196 (2005).
7. I.T. Witting, T.C. Chasapis, F. Ricci, M. Peters, N.A. Heinz, G. Hautier, and G.J. Snyder, *Adv. Electron. Mater.* 5, 1800904 (2019).
8. W. Zhang, K. Zhu, J. Liu, J. Wang, K. Yana, P. Liu, and Y. Wang, *Ceram. Int.* 44, 17251 (2018).
9. D.-B. Zhang, H.-Z. Li, B.-P. Zhang, D.-D. Liang, and M. Xia, *RSC Adv.* 7, 10855 (2017).
10. A. Samarelli, L.F. Llina, S. Cecchi, J. Frigerio, D. Chrastina, G. Isella, E.M. Gubler, T. Etzelstorfer, J. Stangl, Y. Zhanga, M.R. Weaver, P.S. Dobson, and D.J. Paul, *Solid State Electron.* 98, 70 (2014).
11. J. Tani, M. Takahashi, H. Kido, and I.O.P. Conf, Ser. *Mater. Sci. Eng.* 18, 142013 (2011).
12. Y. Du, S.Z. Shen, K. Cai, and P.S. Casey, *Prog. Polym. Sci.* 37, 820 (2012).
13. E.J. Bae, Y.H. Kang, K.S. Jang, and S.Y. Cho, *Sci. Rep.* 6, 18805 (2016).
14. J. Luo, D. Billep, T. Waechter, T. Otto, M. Toader, O. Gordan, E. Sheremet, J. Martin, M. Hietschold, D.R.T. Zahn, and T. Gessnerab, *J. Mater. Chem. A* 1, 7576 (2013).
15. A. Abtahi, S. Johnson, S.M. Park, X. Luo, Z. Liang, J. Mei, and K.R. Graham, *J. Mater. Chem. A* 7, 19774 (2019).
16. R. Kroon, D.A. Mengistie, D. Kiefer, J. Hynynen, J.D. Ryan, L. Yu, and C. Müller, *Chem. Soc. Rev.* 45, 6147 (2016).
17. K.C. See, J.P. Feser, C.E. Chen, A. Majumdar, J.J. Urban, and R.A. Segalman, *Nano Lett.* 10, 4664 (2010).
18. C. Liu, F. Jiang, M. Huang, B. Lu, R. Yue, and J. Xu, *J. Electron. Mater.* 40, 948 (2011).
19. N.S. Ahmed and F. Karaman, *J. Optoelectron. Adv. Mater.* 20, 695 (2018).
20. N.S. Ahmed and F. Karaman, *J. Indian Chem. Soc.* 96, 1199 (2019).
21. T. Mori and T. Nishimura, *J. Solid State Chem.* 179, 2908 (2006).
22. C.C. Chen, Z. Li, L. Shi, and S.B. Cronin, *Nano Res.* 8, 666 (2015).
23. X. Wang, F. Meng, H. Tang, Z. Gao, S. Li, F. Jiang, and J. Xu, *J. Mater. Sci.* 52, 9806 (2017).

24. H. Werheit, *Mat. Sci. Eng. B* 29, 228 (1995).
25. M. Abat, F. Degryse, R. Baird, and M.J. McLaughlin, *J. Plant Nutr. Soil Sci.* 177, 860 (2014).
26. S.D. Mikhailenko, J. Zaidi, and S. Kaliaguine, *J. Chem. Soc., Faraday Trans.* 94, 1613 (1998).
27. M. Mamlouk and K. Scott, *J. Power Sources* 286, 290 (2015).
28. S. Xu, C. Liu, Z. Xiao, W. Zhong, Y. Luo, H. Ou, and J. Wiezorek, *Sol. Energy* 157, 125 (2017).
29. E. Susanti and P. Wulandari, *J. Phys: Conf. Ser.* 1080, 012010 (2018).
30. Y. Xie, S.-H. Zhang, H.-Y. Jiang, H. Zeng, R.-M. Wu, H. Chen, Y.-F. Gao, Y.-Y. Huang, and H.-L. Bai, *Polymers* 19, 61 (2019).
31. T.A. Yemata, Y. Zheng, A.K.K. Kyaw, X. Wang, J. Song, W.S. Chin, and J. Xu, *RSC Adv.* 10, 1786 (2020).
32. B.-W. Park, L. Yang, E.M.J. Johansson, N. Vlachopoulos, A. Chams, C. Perruchot, M. Jouini, G. Boschloo, and A. Hagfeldt, *J. Phys. Chem. C* 17, 22484 (2013).
33. A. El-Ghaffar, A.M. Baraka, M.M. Hefny, E.A. Youssef, and M.M. Aly, *Egypt. J. Chem.* 61, 759 (2018).
34. K. Biswas, in *Spectroscopic Properties of Inorganic and Organometallic Compounds: Volume 45*, ed. by R. Douthwaite, S. Duckett, and J. Yarwood (Royal Society of Chemistry, London, 2014) p. 117.
35. N. Toshima and S. Ichikawa, *J. Electron. Mater.* 44, 384 (2015).
36. S.-M. Kim, C.-H. Kim, Y. Kim, N. Kim, W.-J. Lee, E.-H. Lee, D. Kim, S. Park, K. Lee, J. Rivnay, and M.-H. Yoon, *Nat. Commun.* 9, 1 (2018).
37. C. Dun, C.A. Hewitt, H. Huang, J. Xu, C. Zhou, W. Huang, Y. Cui, W. Zhou, Q. Jiang, and D.L. Carroll, *Nano Energy* 18, 306 (2015).
38. Y. Chen, M. He, B. Liu, G.C. Bazan, J. Zhou, and Z. Liang, *Adv. Mater.* 29, 1604752 (2016).
39. W. Zheng, P. Bi, H. Kang, W. Wei, F. Liu, J. Shi, L. Peng, Z. Wang, and R. Xiong, *Appl. Phys. Lett.* 105, 023901 (2014).
40. S.K. Yee, N.E. Coates, A. Majumdar, J.J. Urban, and R.A. Segalman, *Phys. Chem. Chem. Phys.* 15, 4024 (2013).
41. D. Lee, J. Zhou, G. Chen, and Y. Shao-Horn, *Adv. Electron. Mater.* 5, 1800624 (2019).

Publisher's Note Springer Nature remains neutral with regard to jurisdictional claims in published maps and institutional affiliations.